Title

Multipinhole collimator with 20 apertures for a brain SPECT application

Journal

Medical Physics, 41(11)

ISSN

0094-2405

Authors

Lee, Tzu-Cheng

Ellin, Justin R

Huang, Qiu

et al.

Publication Date

2014-11-01

DOI

10.1118/1.4897567

Peer reviewed

Multipinhole collimator with 20 apertures for a brain SPECT application

Tzu-Cheng Lee and Justin R. Ellin
Physics Research Laboratory, Department of Radiology and Biomedical Imaging, University of California, San Francisco, California 94107

Qiu Huang
School of Biomedical Engineering, Shanghai Jiao Tong University, Shanghai 200030, China

Uttam Shrestha
Physics Research Laboratory, Department of Radiology and Biomedical Imaging, University of California, San Francisco, California 94107

Grant T. Gullberg
Department of Radiotracer Development and Imaging Technology, Life Sciences Division, Lawrence Berkeley National Laboratory, Berkeley, California 94702

Youngho Seo[a)]
Physics Research Laboratory, Department of Radiology and Biomedical Imaging, University of California, San Francisco, California 94107

(Received 27 October 2013; revised 26 August 2014; accepted for publication 15 September 2014; published 14 October 2014)

Purpose: Several new technologies for single photon emission computed tomography (SPECT) instrumentation with parallel-hole collimation have been proposed to improve detector sensitivity and signal collection efficiency. Benefits from improved signal efficiency include shorter acquisition times and lower dose requirements. In this paper, the authors show a possibility of over an order of magnitude enhancement in photon detection efficiency (from 7.6×10^{-5} to 1.6×10^{-3}) for dopamine transporter (DaT) imaging of the striatum over the conventional SPECT parallel-hole collimators by use of custom-designed 20 multipinhole (20-MPH) collimators with apertures of 0.75 cm diameter.
Methods: Quantifying specific binding ratio (SBR) of ^{123}I-ioflupane or ^{123}I-iometopane's signal at the striatal region is a common brain imaging method to confirm the diagnosis of the Parkinson's disease. The authors performed imaging of a striatal phantom filled with aqueous solution of I-123 and compared camera recovery ratios of SBR acquired between low-energy high-resolution (LEHR) parallel-hole collimators and 20-MPH collimators.
Results: With only two-thirds of total acquisition time (20 min against 30 min), a comparable camera recovery ratio of SBR was achieved using 20-MPH collimators in comparison to that from the LEHR collimator study.
Conclusions: Their systematic analyses showed that the 20-MPH collimator could be a promising alternative for the DaT SPECT imaging for brain over the traditional LEHR collimator, which could give both shorter scan time and improved diagnostic accuracy. © *2014 American Association of Physicists in Medicine.* [http://dx.doi.org/10.1118/1.4897567]

Key words: multipinhole SPECT, brain SPECT, DAT imaging, 123I-ioflupane

1. INTRODUCTION

Parkinson's disease (PD) is a progressive neurological disorder that affects the function of human brain cells, neurons.[1] For the purposes of proper therapeutic treatment, it is crucial to differentiate PD from other movement related disorders (e.g., essential tremor, drug-induced Parkinsonism) given their different prognoses. The clinical diagnostic tests are normally based on the motor symptoms such as tremor, rigidity and slowness of movement, inferences which are based on cognitive and neurobehavioral problems, sensory and sleep difficulties, and patient's medication responses.[2–5] Several imaging methods have been proposed and are being investigated for diagnostic confirmation of the PD at an early stage of the disease progression.[6–8]

^{123}I-ioflupane (FP-CIT, DaTSCAN, GE Healthcare, UK) and ^{123}I-iometopane (β-CIT, DOPASCAN, MAP Medical Technologies Oy, Finland) are two commercially available single photon emission computed tomography (SPECT) imaging agents that have been used in cases of suspected PD.[9–11] *Ioflupane* and *iometopane* are drugs with high binding affinity to the dopamine transporter (DaT) found at the presynaptic region of the neurons of the subcortical region of the forebrain (striatum). Since DaT concentrations are lower in presynaptic parkinsonian neurons, the PD patients show a relatively lower I-123 labeled *Ioflupane* or *iometopane* uptake, and an efficient and accurate imaging may confirm the PD diagnosis.

Low-energy high-resolution (LEHR) parallel hole is the most commonly used collimator for SPECT DaT imaging.

LEHR collimator was first introduced in 1964 as a replacement for the original single pinhole collimator for greater improvements in imaging efficiency.[12] An early LEHR parallel-hole collimator design achieved an efficiency of 2.57 $\times 10^{-4}$ and a resolution of 1.5 cm at 10 cm.[12] Surprisingly, around 50 years later, current LEHR designs with the clinically used SPECT scanner achieved very little improvement in either efficiency (~1.7–1.8$\times 10^{-4}$) or resolution (~0.7 –1.0 cm FWHM at 10 cm).[13,14] Based on the package insert of DaTscan (GE Healthcare), a minimum of 1.5 million total counts is needed in order to achieve optimal image quality. In other words, for a LEHR collimator mounted conventional dual-headed SPECT scanner with recommended activities of I-123 (~185 MBq), it usually requires 30–45 min to finish a single scan. Efforts have been made to use a converging geometry such as fan-beam or cone-beam for the collimator design for brain SPECT in order to obtain improved spatial resolution with same or improved sensitivity for small regions of interest. Certain highly optimized designs for cone-beam collimation with shorter septa, longer holes, and short focal lengths have achieved gains in signal-to-noise ratio (SNR) of 1.0–3.5 [periphery vs center of the field of view (FOV)] over conventional parallel-hole LEHR collimation.[15]

Pinhole systems can offer improvements in spatial resolution over traditional LEHR parallel-hole SPECT through the use of magnification factors, but at the cost of detection efficiency.[16] Multipinhole systems compensate for this decreased sensitivity by projecting the desired volume of interest multiple times on the detector when the object is much smaller than the gamma camera detector area. However, there is also a trade-off in using multipinhole collimators since the magnification factor is typically diminished in comparison to that of a single pinhole system. A few theoretical calculations and simulation studies for the multipinhole collimator on brain imaging applications have shown its potential to achieve much better signal efficiency through high photon detection efficiency than the traditional LEHR parallel-hole configuration.[17–20] Multipinhole imaging has been used as early as 1978 (Ref. 21) and become more popular recently within small animal imaging;[22–27] the success of the latter generated significant interest to a generalization of these systems to humans. In our recent study inspired by an earlier work by Funk,[28] we reported the performance test of the multipinhole collimation and showed that the new 20-pinhole collimator improves the SNR of myocardial perfusion imaging (MPI) by a factor greater than 2 over that of using LEHR collimators with a fixed resolution of 12.5 mm.[29]

The purpose of this study was to investigate the performance of a new 20 multipinhole (20-MPH) collimator over the conventional LEHR technology for brain SPECT imaging and to perform physical experimental measurements with the 20-MPH. Our working hypothesis was that a substantial improvement in counting statistics (signal-to-noise, efficiency, etc.) would improve brain SPECT DaT imaging when a LEHR collimator was replaced with a 20-MPH collimator in a commonly used clinical SPECT camera (Fig. 1). We investigated if a comparable specific binding ratio (SBR) measurement of the striatal phantom could be achieved with reduced total acquisition time compared to the imaging scenario using the conventional LEHR parallel-hole collimator through comparison of the SNR and calculation of the SBR. Furthermore, for the application of DaT SPECT imaging, we wanted to test if the 20-MPH collimator could also perform better camera recovery ratios (CRRs) for a given SBR with a shorter acquisition time. The CRR here is the ratio of the measured SBR (after reconstruction) to the known SBR from the tracer distribution in the phantom. Reduced scan times would have a significant impact on patient comfort and throughput and may pave the way toward dose-reduction in brain SPECT imaging.

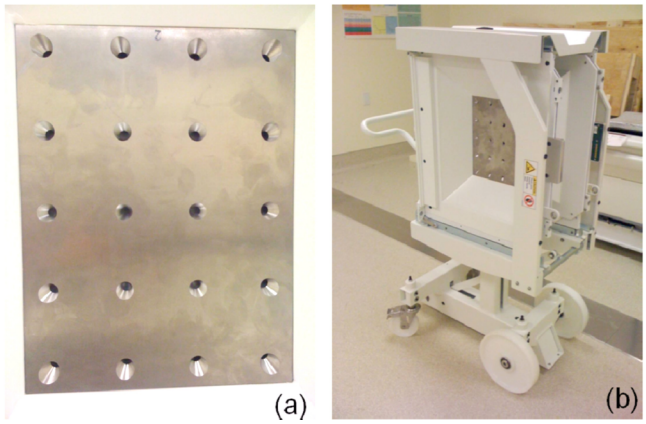

FIG. 1. (a) Tungsten 20-pinhole aperture plate. (b) Assembled with collimator mount for use with a dual-head clinical SPECT scanner (GE Infinia Hawkeye 4).

During the course of the study, pixel-based ordered subset expectation maximization (OSEM) was used for image reconstruction of the 20-MPH for potential speedup in clinical settings and provided an opportunity to validate this relatively recent reconstruction algorithm with experimental data.

2. MATERIALS AND METHODS

2.A. Theoretical calculation for the performance of 20-MPH

Motivation for the selection of the parameters of the 20-MPH and the study were to match conventional LEHR based on theoretical calculations of the ideal efficiency (E) and system resolution (R_s) for the 20-MPH collimator estimated as for a point source at the focal point[17,30]

$$E = N_p \varepsilon \frac{D^2 + \frac{2}{\mu} D \tan\left(\frac{\alpha}{2}\right) + \frac{2}{\mu^2} \tan^2\left(\frac{\alpha}{2}\right)}{16 r_c^2}, \tag{1}$$

$$R_S = \sqrt{\left(\frac{r_c R_i}{r_c - r_d}\right)^2 + \left(\frac{r_d \left(D + \ln 2 \tan\left(\frac{\alpha}{2}\right)/\mu\right)}{r_c - r_d}\right)^2}, \tag{2}$$

$$E = \frac{N_p \varepsilon}{16 r_c^2} \left[\left(\frac{R_s}{r_d} \sqrt{\left[(r_c - r_d)^2 - (r_c R_i)^2\right]} + a(\ln 2 - 1) \right)^2 + \frac{1}{4} a^2 \right], \tag{3}$$

where $a = 2/\mu(\tan(\alpha/2))$, "$\varepsilon$" is the capture efficiency of the detector, "D" is the diameter of the single pinhole, "μ" is the attenuation coefficient of the pinhole material, "α" is the pinhole opening angle, and "r_d" and "r_c" are detector and collimator radius of rotation (ROR), respectively. The intrinsic resolution of the detector is denoted by "R_i." By eliminating the pinhole diameter (D) from Eqs. (1) and (2), one can also obtain the correlation between E and R_s in Eq. (3).

In this study, we used a custom-designed multipinhole cone-beam collimator made up of tungsten pinholes in a 0.8 cm thick sheet with the frame dimensions of 36×27 cm^2 (Fig. 1). The 20 pinholes, N_p, each with 0.75 cm aperture diameter are arranged such that the distances between pinhole centers are 6.2 and 5.8 cm for the columns and rows, respectively. The tilt axis of all pinholes pass through a common point located at 39 cm perpendicular to the center of the detector surface giving a range of tilt angles from 6.2° to 29.4° to the normal. The collimator was mounted on the dual-head SPECT/CT system (GE Infinia Hawkeye 4). The maximum detector ROR of the gamma camera, $r_{d,\max}$, was 31.5 cm. The detector ROR and collimator ROR were set as 31.5 and 19.3 cm, respectively. The intrinsic resolution of the detector, R_i, from the vendor's datasheet was 0.38 cm.[31] The opening angle (α) of the knife-edge pinholes for a 10.5 cm radius of FOV was set to 65.4°, large enough to contain the whole brain region. The 20-MPH collimator allows for multiple simultaneous angular projections with each stop over the entire detector area with minimum overlaps.

The theoretical performance of the 20-MPH collimator can be assessed from Eqs. (1) and (2). The capture efficiency, ε, of the gamma camera with the crystal layer thickness of 0.95 cm was 80%,[31] and the attenuation coefficient (μ) of tungsten for 158 keV gamma ray (I-123) was 30.43 cm^{-1}. For the parameters used in this report, the ideal signal efficiency of 1.6×10^{-3} and the resolution of 2.06 cm could be expected. Ideally, this efficiency is 22 times better than LEHR (7.2×10^{-5}) with only 2.8 times system resolution loss (0.74 cm).

2.B. Experimental setups, image acquisitions and reconstructions

All image acquisitions were done with a GE Infinia Hawkeye 4 dual-head SPECT/CT scanner (Chalfont St. Giles, UK) with the camera operating in H-mode. The dimensions of the single projected image were 128×128 pixels with pixel size of 0.442 cm and were all reconstructed in $128\times128\times128$ voxels with a voxel size of 0.368 cm^3 (1.2 zoom-in factor was applied). The collimator ROR was set to be 22.5 cm for LEHR and 19.3 cm for 20-MPH collimators with circular orbits. The distance of these RORs were chosen to be as close to the phantom as possible while allowing the gantry clearance of the patient table. A head-holder was not available for this study, which would have allowed for a smaller ROR. The LEHR parallel-hole collimator used had hexagonal holes with 1.5 mm diameter of length 35 mm and 0.2 mm septal thickness.[31] Projections were triple-energy window (TEW) scatter corrected.[32] Since duplicating the same experimental conditions is difficult to realize, multiple noise realizations for the 20-MPH collimator were simulated by adding Poisson noise to the experimental projections using the pixel values of the measured data set as the actual mean prior to reconstruction. Image reconstruction was performed for both collimators using a patient-specific system matrix generated from coregistered CT data. The system matrix incorporates the number of views, the angles of rotations, collimator hole geometry, and patient anatomy (from the CT-generated attenuation map) explicitly. The effects of scatter and parallax were not included in the system matrix.[29] Finally, all reconstructed images were postprocessed with a low-pass order 10 Butterworth filter with 0.7 cycles per pixel (pixel size of 0.368 cm) as previously suggested[9,10] and to match the postfiltering used in the vendor provided software for LEHR OSEM reconstruction of the brain. This postfilter helps to remove high frequency noise that may be a result of the acquisition or reconstruction.

The striatal phantom (Radiology Support Devices, Long Beach, CA) was prepared using 59 kBq/ml of aqueous solution of I-123 for left striatum, 37 kBq/ml for right striatum with 4.1 kBq/ml for the background brain shell. A total of 6.2 MBq of radioactivity were set in this phantom in order to mimic the approximately 3%–4% of total injected radioactivity (185 MBq) distributed in brain for 5 h after the injection.[33] Thus, the SBR of I-123 were set as 14.4:1 (L) and 9:1 (R). One hundred and twenty 30-s projections (60 stops) were acquired for the LEHR data, and images were iteratively reconstructed with two iterations of OSEM (ordered subset expectation maximization, 10 subsets)[34] as implemented in the vendor-supplied software used in clinical protocols at our scanner for Brain imaging at USCF. No resolution modeling was included in the OSEM algorithm for LEHR reconstruction. Eight 300-s projections (4 stops) were acquired over 360° for the 20-MPH data. Given the number of stops and pinholes, issues may arise in the use of OSEM to provide sufficient angles and counts to each subset. The projections from 20-MPH scan were reconstructed with 240 iterations of maximum-likelihood expectation maximization (MLEM)[35] or with equal scalar product of subset and iteration numbers of pixel-based OSEM (POSEM, 8 subsets 30 iterations and 16 subsets 15 iterations). Pixel-based OSEM generates subsets by regular patterning of the detector pixels in each projection instead of over entire projection angles. Subsets are chosen to be as spaced as far as possible from other subsets. Such a choice of subsets ensures a more evenly distributed share of counts between subsets and sufficient angular sampling for all subsets when compared to OSEM.[36]

2.C. The voxel-based SBR measurements and SNR

In order to measure the SBR, a voxel-based semiquantitative method as described by Tossici-Bolt *et al.*[37] was used

$$\mathrm{SBR}_{\mathrm{measured}} = \left(\frac{1}{V_s}\right)\left\{\frac{Ct_{\mathrm{VOI}}}{C_r} - V_{\mathrm{VOI}}\right\}. \quad (4)$$

Here, V_s is the total physical volume of the striatum, C_r is the number of counts within a reference region, Ct_{VOI} is the total

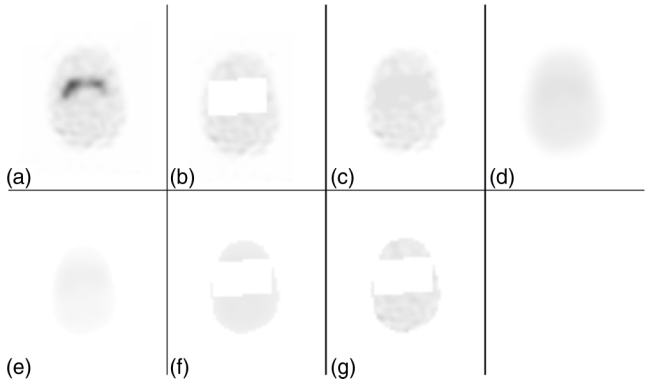

FIG. 2. Illustration of the process by which the SBR and SNR are calculated for the 20-MPH. (a) Original image. (b) The striatal VOIs were chosen to cover both striata. (c) The image is smoothed to remove statistical variation and all voxels brighter than M_{ns} in the VOI replaced with M_{ns}. (d) The image is heavily filtered to generate a smooth contour. (e) A threshold boundary is generated with $0.5M_{ns}$ to remove partial volume effects associated with the outside of the head. (f) The final image used to estimate the nonspecific binding in all regions of the head. (g) The threshold boundary and the striatal VOIs are used as a mask in (a) to create the region for the calculation of the noise in the SNR of Eq. (5).

number of counts within a boxlike VOI that contains both striata, and V_{VOI} is the volume of that VOI. The purpose of the method, summarized in Fig. 2, is to segment and separate the reference region from the "active" region containing the striata. Filters and thresholds are applied to remove noise since it is assumed that the nonspecific binding is the same in all regions as well as to isolate the contour of the head which is prone to partial volume effects. The VOI was first generated from two smaller VOIs each of $6.1\times4.8\times4.4$ cm^3 placed in the image to fully cover the left and right striata. Second, the reference region (all regions outside the VOI) was smoothed (Gaussian, 5×5, 0.5 pixel S.D.) three times. Third, all voxels within the VOI brighter than the brightest pixel within the reference region, M_{ns}, were replaced with M_{ns} and the image smoothed again (Gaussian, 5×5, 0.5 pixel S.D., 20 times). Next, pixels with values half of M_{ns} in the image were set as the boundary threshold of the brain shell in order to get the volume and the signal intensity of the reference region, thus the signal concentration of reference (C_r) could be determined. Finally, Eq. (4) was used for calculating the SBR.[37] The total volume of the striatum here in the phantom was set to be 11.4 ml, and all image-processing steps described above were run on the MATLAB software (MathWorks, Natick, MA).

The CRR was used to evaluate the DaT scan performance on two collimators

$$\text{Camera recovery ratio} = \frac{\text{SBR}_{\text{measured}}}{\text{SBR}_{\text{ideal}}}. \quad (5)$$

Here, $\text{SBR}_{\text{measured}}$ is the SBR calculated from the reconstructed images and $\text{SBR}_{\text{ideal}}$ is set to the concentrations set during phantom preparation.

The SNR was used as a noise metric for the two collimators

$$\text{SNR} = \frac{\bar{C}_{\text{VOI}}}{\sigma_b}. \quad (6)$$

Here, $\bar{C}_{\text{VOI}}$ is the mean number of counts within the reference region of the original reconstructed image using the generated isocontour and striatal VOIs as image masks [Figs. 2(e) and 2(g)] and σ_b is the standard deviation of the counts in that region. In our phantom, the volume for the nonspecific binding is homogeneous and uniform with statistical variation attributable to noise alone.

3. RESULTS

3.A. Reconstructed striatal images

For experimental test on a striatal phantom, as the control group, a 30-min total acquisition time with 60 stops and 120 views standard LEHR acquisition was set. The data were reconstructed using the vendor-packed OSEM software. In Fig. 3(a), we show the central transverse slice of the reconstructed image. As expected, the striata with high signal intensity in the left and low intensity in the right are clearly recognized for the 14.4:1 (L) and 9:1 (R) SBR setting. The same striatal

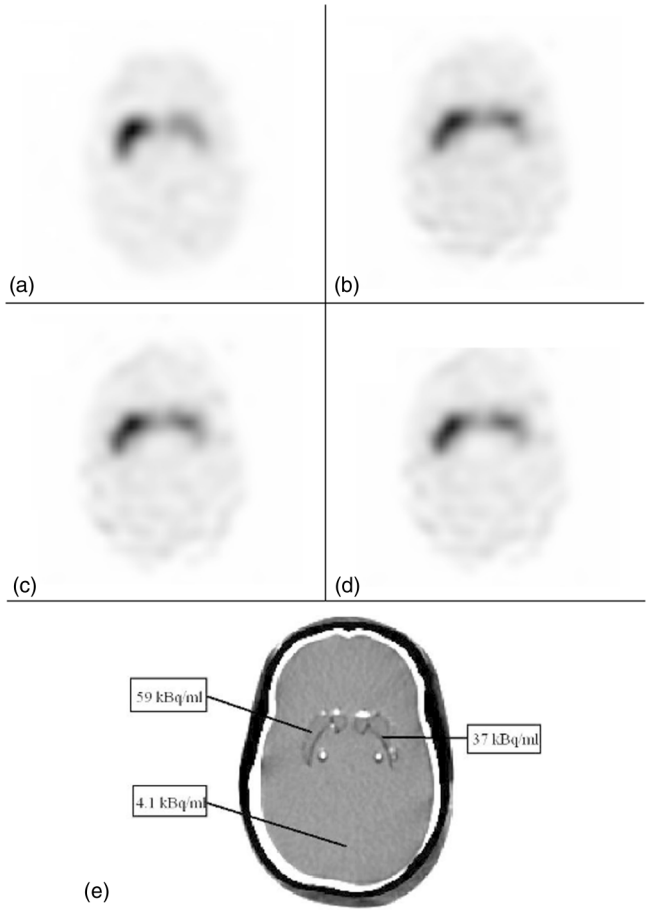

FIG. 3. Reconstructed striatal phantom I-123 images with 14.4:1 (L) and 9:1 (R) SBR setting. (a) Acquired with conventional LEHR collimator for 30 min and 120 total views and reconstructed with OSEM (10 subset, 2 iterations). Acquired with 0.75 cm aperture 20-MPH collimator for 20 min and 8 total views, (b) reconstructed with 240-iterative MLEM, (c) 8 subsets, 30 iterations POSEM, and (d) 16 subsets, 15 iterations POSEM. (e) CT image of the striatal phantom with arrows indicating radionuclide concentration distribution. The two small circles are vinyl screws.

phantom image with shorter total acquisition time (20 min, 4 stops) was acquired with 20-MPH collimator with aperture size 0.75 cm, and the data were further reconstructed with the standard MLEM or POSEM. Figures 3(b)–3(d) show reconstructed images with 240 iterations of MLEM, 30 iterations of 8-subset POSEM, and 15 iterations of 16-subset POSEM, respectively. The relative signal contrasts of right striatum in all 20-MPH images seem to be enhanced as compared to that of the LEHR image. In addition to this, we also noticed that the choice of the number of subset does not seem to affect visual appearance of the images. However, if we compare 20-MPH with LEHR-images or the CT data in Fig. 3(e), some morphological differences on the shape as well on the structure of the striata can be visible.

3.B. Specific binding ratio, camera recovery ratios, and SNR

We further quantified the SBR and SNR from different collimators and reconstruction algorithms; the results are listed in Table I with the camera recovery ratio defined as in Eq. (5). For the 30-min LEHR acquisition, the recovery ratios were found to be 80.7% (L) and 75.6% (R). For the same phantom with 20-MPH collimator and a two-third acquisition time, the recovery ratios were around 79.4%–83.0% (L) and 74.4%–80.4% (R) when different image reconstruction methods were applied. The deviation of the measured SBR values from the known concentrations for the LEHR collimator was 10.6%, with errors of 2.1%, 8.9%, and 12.4% for 20-MPH acquisitions; the errors from 20-MPH were positively dependent on the reconstruction acceleration factors (see Table I). The SNR was found to be 2.7 for the LEHR acquisition, and the values for the 20-MPH found to be around 4.7.

The values listed above in Table I are those calculated from the experimental data. The same size ROI was used in the reconstructions with each algorithm. The SBR was then calculated for ten noisy data sets, and the mean and the standard deviation of those values were calculated to estimate the signal error due to noise. The SNR was used as a metric to distinguish noise performance of the collimators themselves. Figures 4(a) and 4(b) show images with the reconstruction performed with 240 iterations of MLEM and 8 subsets, 30 iterations of OSEM, respectively. Similarly, Figs. 4(c) and 4(d) show reconstructed images with added Poisson noise on the projection data. All images are before application of the postfilter prior to the SBR quantification measurement. Visually, the images have little variation with the most noticeable differences being in the nonstriatal regions. Error attributable to noise is significantly less than the variation in SBR mean values between different reconstruction algorithms. The overestimation of the SBR for the Left Striatum and the underestimation of the SBR for the Right Striatum for POSEM are likely artifacts of the algorithm with implications for speed up in clinical use.

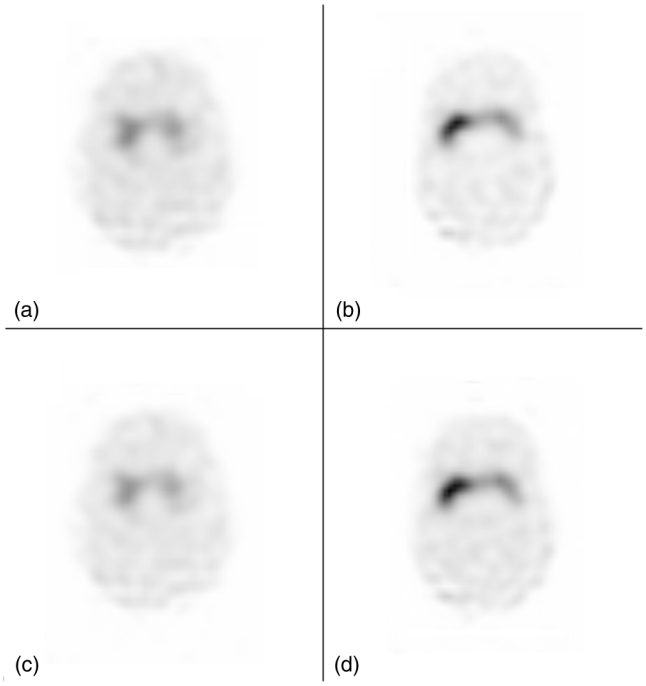

FIG. 4. Reconstructed prefiltered striatal phantom I-123 images with 14.4:1 (L) and 9:1 (R) SBR setting. Acquired with 0.75 cm aperture 20-MPH collimator for 20 min and 8 total views, (a) reconstructed with 240-iterative MLEM, (b) 8 subsets, 30 iterations POSEM. Images constructed from noisy projections with (c) 240-iterative MLEM, (d) 8 subsets, 30 iterations POSEM.

4. DISCUSSION

DaTSCAN and DOPASCAN are two commercially available drugs widely used for evaluating presynaptic dopami-

TABLE I. The SBRs, camera recovery ratios, and SNR values of striatal-phantom images measured by the LEHR or 20-MPH collimator. All SNR values have a standard deviation of ±0.1.

	Left Striatum SBR_{ideal}: 14.4:1		Right Striatum SBR_{ideal}: 9:1		
Tossici-Bolt's method for quantifying SBR	$SBR_{measured}$	CRR (%)	$SBR_{measured}$	CRR (%)	SNR
Total acquisition time: 30min; Projection: 120 views					
LEHR, OSEM 10 sub., 2 it.	11.62	80.7	6.80	75.6	2.7
Total acquisition time: 20min; Projection: 8 views					
20-MPH, MLEM 240 it.	11.44 ± 0.01	79.4	7.24 ± 0.02	80.4	4.7
20-MPH, POSEM 8 sub. 30 it.	11.74 ± 0.03	81.5	7.07 ± 0.06	78.6	4.7
20-MPH, POSEM 16 sub. 15 it.	11.58 ± 0.05	80.4	6.70 ± 0.04	74.4	4.6

nergic system,[9,10] and can be used for differentiating Parkinson's disease patients (DaT disorder in presynaptic neurons) from other motion-disorder patients by measuring the specific binding ratio of radioactive agent at the striatal region. Therefore, we expect that the higher and steady value of camera recovery ratio of SBR could lead to more accurate differentiation of high- and low-SBR. This would help physicians provide appropriate treatments to the potential patient at an early stage of disease development.

The SBR measurement for 20-MPH was comparable to that of LEHR with better noise performance despite a slight degradation in image resolution. The small deviation of the SBR measurements is not surprising given the repeated application of postfiltering and suggests that for a single collimator and algorithm, the SBR measurement is relatively independent of noise. The difference between the SBR values for LEHR and 20-MPH is likely due to partial volume effects that are a consequence of resolution loss but translate to a variance of a few percent. However, the SNR of 20-MPH is significantly higher than that of LEHR independent of the different reconstruction algorithms we applied. SNR depends also on reconstruction parameters (iterations and subsets) and resolution modeling (not used in LEHR OSEM), and further study is needed to optimize these settings and compare collimator performance. This feature could make 20-MPH collimator, which offered a superior efficiency performance with little resolution loss, an ideal alternative over LEHR collimator for the DaT brain SPECT imaging. However, it should be noted that care should be taken when the imaging task relies on image resolution such as in delineating the shape of striatal structures, as the 20-MPH slightly distorts these shapes especially when higher acceleration factors (for example, higher subsets for POSEM) are applied in reconstruction.

The camera recovery ratios with the 20-MPH collimator were still comparable to those in LEHR even when a high-accelerated reconstruction algorithm was applied (e.g., POSEM, 16 subset) (Table I). The 20-MPH could be a promising alternative for solving the demand of high-sensitivity-required SPECT imaging in the near future.

5. CONCLUSION

In this study, we introduced a 20 multipinhole collimator compatible with commercially available SPECT systems for a brain SPECT application (DaTscan imaging). We demonstrated higher detection efficiency and comparable SBR measurement with improved noise performance of 20-MPH collimators in comparison to those of conventional LEHR with only two-third of the total acquisition time for comparable image qualities.

ACKNOWLEDGMENTS

This work was supported in part by National Heart, Lung and Blood Institute under Grant No. R21 HL083073 (J.D.B. and Y.S.) and Grant No. R01 HL050663 (J.E., U.S., G.T.G., and Y.S.), and National Institute of Biomedical Imaging and Bioengineering under Grant No. R01 EB012965 (T.-C.L. and Y.S.).

[a]Author to whom correspondence should be addressed. Electronic mail: youngho.seo@ucsf.edu

[1]O. Hornykiewicz, "Dopamine (3-hydroxytyramine) and brain function," Pharmacol. Rev. **18**, 925–964 (1966).
[2]J. Jankovic, "Parkinson's disease: Clinical features and diagnosis," J. Neurol., Neurosurg. Psychiatry **79**, 368–376 (2008).
[3]A. J. Hughes, S. E. Daniel, L. Kilford, and A. J. Lees, "Accuracy of clinical diagnosis of idiopathic Parkinson's disease: A clinico-pathological study of 100 cases," J. Neurol. Neurosurg. Psychiatry **55**, 181–184 (1992).
[4]A. J. Hughes, Y. Ben-Shlomo, S. E. Daniel, and A. J. Lees, "What features improve the accuracy of clinical diagnosis in Parkinson's disease: A clinicopathologic study," Neurology **57**, S34–S38 (1992).
[5]D. B. Calne, B. J. Snow, and C. Lee, "Criteria for diagnosing Parkinson's disease," Ann. Neurol. **32**, S125–S127 (1992).
[6]K. Badiavas *et al.*, "SPECT imaging evaluation in movement disorders: Far beyond visual assessment," Eur. J. Nucl. Med. Mol. Imaging **38**, 764–773 (2011).
[7]A. J. Stoessl, W. W. Martin, M. J. McKeown, and V. Sossi, "Advances in imaging in Parkinson's disease," Lancet Neurol. **10**, 987–1001 (2011).
[8]J. J. Frost *et al.*, "Positron emission tomographic imaging of the dopamine transporter with 11C-WIN 35,428 reveals marked declines in mild Parkinson's disease," Ann. Neurol. **34**, 423–431 (1993).
[9]J. Darcourt *et al.*, "EANM procedure guidelines for brain neurotransmission SPECT using (123)I-labelled dopamine transporter ligands, version 2," Eur. J. Nucl. Med. Mol. Imaging **37**, 443–450 (2010).
[10]D. S. Djang *et al.*, "SNM practice guideline for dopamine transporter imaging with 123I-ioflupane SPECT 1.0," J. Nucl. Med. **53**, 154–163 (2012).
[11]G. Healthcare, DaTscan prescribing information, 2011.
[12]H. O. Anger, "Scintillation camera with multichannel collimators," J. Nucl. Med. **5**, 515–531 (1964).
[13]M. N. Wernick and J. N. Aarsvold, *Emission Tomography* (Elsevier Academic Press, San Diego, CA, 2004).
[14]A. Giussani and C. Hoeschen, *Imaging in Nuclear Medicine* (Springer-Verlag, Berlin Heidelberg, 2013).
[15]M. A. Park, S. C. Moore, and M. F. Kijewski, "Brain SPECT with short focal-length cone-beam collimation," Med. Phys. **32**, 2236–2244 (2005).
[16]R. J. Jaszczak, J. Li, H. Wang, M. R. Zalutsky, and R. E. Coleman, "Pinhole collimation for ultra-high-resolution, small-field-of-view SPECT," Phys. Med. Biol. **39**, 425–437 (1994).
[17]M. C. Goorden, M. C. Rentmeester, and F. J. Beekman, "Theoretical analysis of full-ring multi-pinhole brain SPECT," Phys. Med. Biol. **54**, 6593–6610 (2009).
[18]R. K. Rowe *et al.*, "A stationary hemispherical SPECT imager for three-dimensional brain imaging," J. Nucl. Med. **34**, 474–480 (1993).
[19]W. P. Klein *et al.*, *1995 IEEE Nuclear Science Symposium and Medical Imaging Conference Record* (IEEE, San Francisco, CA, 1995), Vol. 2, pp. 931–933.
[20]M. M. Rogulski, H. B. Barber, H. H. Barrett, R. L. Shoemaker, and J. M. Woolfenden, "Ultra-high-resolution brain SPECT imaging: Simulation results," IEEE Trans. Nucl. Sci. **40**, 1123–1129 (1993).
[21]R. A. Vogel, D. Kirch, M. LeFree, and P. Steele, "A new method of multiplanar emission tomography using a seven pinhole collimator and an Anger scintillation camera," J. Nucl. Med. **19**, 648–654 (1978).
[22]Z. Cao, G. Bal, R. Accorsi, and P. D. Acton, "Optimal number of pinholes in multi-pinhole SPECT for mouse brain imaging—A simulation study," Phys. Med. Biol. **50**, 4609–4624 (2005).
[23]J. Nuyts, K. Vunckx, M. Defrise, and C. Vanhove, "Small animal imaging with multi-pinhole SPECT," Methods **48**, 83–91 (2009).
[24]F. van der Have *et al.*, "U-SPECT-II: An ultra-high-resolution device for molecular small-animal imaging," J. Nucl. Med. **50**, 599–605 (2009).
[25]K. Vunckx, D. Beque, M. Defrise, and J. Nuyts, "Single and multipinhole collimator design evaluation method for small animal SPECT," IEEE Trans. Med. Imaging **27**, 36–46 (2008).
[26]K. Vunckx, P. Suetens, and J. Nuyts, "Effect of overlapping projections on reconstruction image quality in multipinhole SPECT," IEEE Trans. Med. Imaging **27**, 972–983 (2008).

[27]F. Beekman and F. Have, "The pinhole: Gateway to ultra-high-resolution three-dimensional radionuclide imaging," Eur. J. Nucl. Med. Mol. Imaging **34**, 151–161 (2006).
[28]T. Funk, D. L. Kirch, J. E. Koss, E. Botvinick, and B. H. Hasegawa, "A novel approach to multipinhole SPECT for myocardial perfusion imaging," J. Nucl. Med. **47**, 595–602 (2006).
[29]J. D. Bowen *et al.*, "Design of 20-aperture multipinhole collimator and performance evaluation for myocardial perfusion imaging application," Phys. Med. Biol. **58**, 7209–7226 (2013).
[30]S. D. Metzler, J. E. Bowsher, M. F. Smith, and R. J. Jaszczak, "Analytic determination of pinhole collimator sensitivity with penetration," IEEE Trans. Med. Imaging **20**, 730–741 (2001).
[31]G. Healthcare, InfiniaTM HawkeyeTM 4 Product Datasheet, 2006.
[32]K. Ogawa, Y. Harata, T. Ichihara, A. Kubo, and S. Hashimoto, "A practical method for position-dependent Compton-scatter correction in single photon emission CT," IEEE Trans. Med. Imaging **10**, 408–412 (1991).
[33]J. Booij *et al.*, "Human biodistribution and dosimetry of [123I]FP-CIT: A potent radioligand for imaging of dopamine transporters," Eur. J. Nucl. Med. **25**, 24–30 (1998).
[34]H. M. Hudson and R. S. Larkin, "Accelerated image reconstruction using ordered subsets of projection data," IEEE Trans. Med. Imaging **13**, 601–609 (1994).
[35]L. A. Shepp and Y. Vardi, "Maximum likelihood reconstruction for emission tomography," IEEE Trans. Med. Imaging **1**, 113–122 (1982).
[36]W. Branderhorst, B. Vastenhouw, and F. J. Beekman, "Pixel-based subsets for rapid multi-pinhole SPECT reconstruction," Phys. Med. Biol. **55**, 2023–2034 (2010).
[37]L. Tossici-Bolt, S. M. Hoffmann, P. M. Kemp, R. L. Mehta, and J. S. Fleming, "Quantification of [123I]FP-CIT SPECT brain images: An accurate technique for measurement of the specific binding ratio," Eur. J. Nucl. Med. Mol. Imaging **33**, 1491–1499 (2006).